



FACULTÉ DES SCIENCES APPLIQUÉES

Identifying and Simulating Nonlinearities in a 2-DoF Mechanical System

NONLINEAR VIBRATION STRUCTURE OF AEROSPACE STRUCTURES
2024-2025

Authors:

Victor Renkin
Félix Weis

ID :

s2306326
s201629

12th December 2024



Contents

1	Introduction	2
1.1	System Description	2
2	Identification of the Nonlinearity	3
2.1	Detection of Nonlinearity	3
2.2	Characterization of Nonlinearity	5
2.2.1	Determine the Nonlinearity Location	5
2.2.2	Acceleration Surface Method (ASM)	5
2.3	Parameter Estimation	8
3	Simulation of the Nonlinearity	10
3.1	Nonlinear Frequency Responses (NLFRs)	10
3.1.1	NLFRs Calculation	10
3.1.2	NLFRs Representation	11
3.1.3	NLFRs Validation	12
3.2	Nonlinear Normal Modes (NNMs)	14
3.2.1	Backbone Curve	14
4	Conclusion	16
A	Experimental Setup Parameters	17
A.1	Experimental 1	17
A.2	Experimental 2	17
A.3	Experimental 3	18



1 Introduction

Nonlinearities are critical in modern engineering, especially in aerospace and mechanical structures, where they often arise due to large displacements, material properties, friction, or complex boundary conditions [10]. These nonlinear effects can significantly alter a system behavior, leading to phenomena such as shifts in resonance frequencies or the emergence of unexpected resonances. Understanding and accounting for these behaviors is essential for designing reliable and efficient systems.

This project aims to address the challenge of identifying and simulating nonlinearities in a two-degree-of-freedom system. The identification process involves three main steps: detection, to establish whether nonlinearity is present in the system this is made by looking at the measurement; characterization, to determine its specific features and locate where it occurs this is made; and parameter estimation using *Acceleration Surface method* (ASM), to quantify the nonlinear terms governing the system's behavior this is made by using the *Restoring Force Surface* (RFS) method. After completing these steps, the system is reconstructed to incorporate the identified nonlinearities for further simulation.

Once the nonlinear behavior is characterized, the system is simulated under nonlinear conditions using a combination of the shooting algorithm and sequential continuation. Nonlinear Frequency Responses (NLFRs) are analyzed for various excitation amplitude, validated against experimental measurements obtained through upward and downward sine sweeps. Additionally, the Nonlinear Normal Modes (NNMs) are explored to extract backbone curves and investigate their relationship with NLFRs. These insights offer a comprehensive understanding of the system's nonlinear dynamics and provide a basis for further refinement and application.

1.1 System Description

The mass, linear stiffness, and linear damping matrices are provided in the project statement and are given as follows:

$$\mathbf{M} = \begin{bmatrix} 1 & 0 \\ 0 & 1 \end{bmatrix}, \quad \mathbf{C} = \begin{bmatrix} 3 & -1 \\ -1 & 3 \end{bmatrix}, \quad \mathbf{K} = \begin{bmatrix} 2 \times 10^4 & -1 \times 10^4 \\ -1 \times 10^4 & 2 \times 10^4 \end{bmatrix}. \quad (1.1)$$

Nonlinearities, with their mathematical forms and coefficients, can manifest anywhere in the system. The linear system can be represented as a two-degree-of-freedom mass-spring-damper system, as illustrated in Figure 1.1.

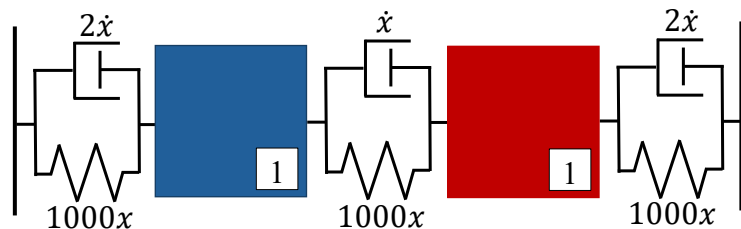


Figure 1.1: Linear diagram based on Equation 1.1.

In the absence of nonlinearity, this system has two resonance frequencies: $f_1 = 15.92$ Hz and $f_2 = 27.57$ Hz; with corresponding damping factors are $\xi_1 = 1\%$ and $\xi_2 = 1.2\%$.



2 Identification of the Nonlinearity

The identification process may be regarded as a progression through three main steps, namely detection, characterization, and parameter estimation, as outlined in Figure 2.1

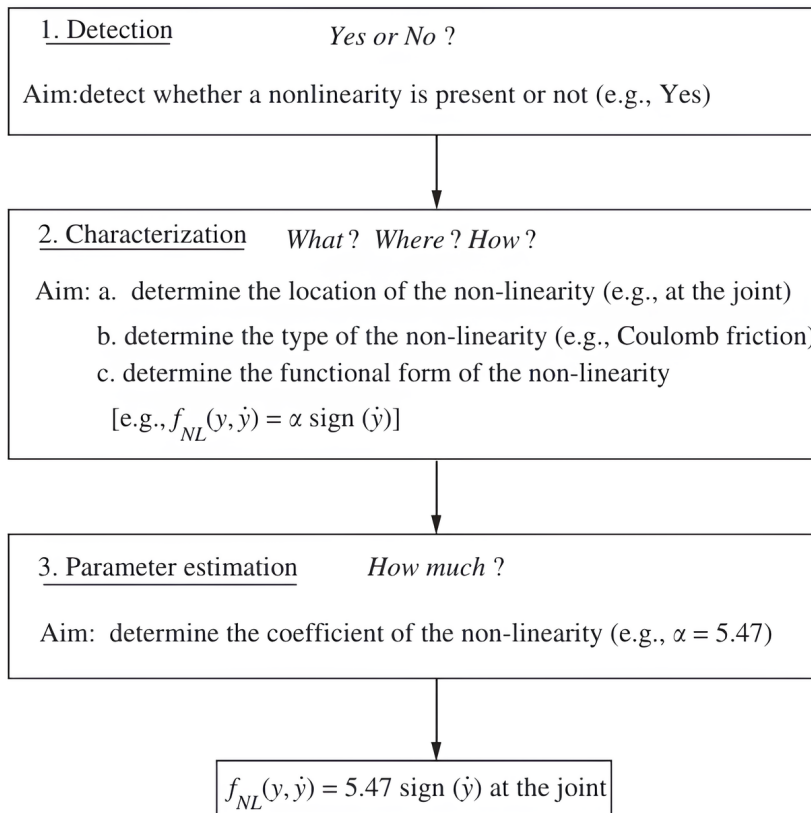


Figure 2.1: Process for identifying nonlinearity [10].

Once nonlinear behavior has been detected, providing compelling evidence that the structure behaves nonlinearly, the next step is to characterize the nonlinearity by locating all nonlinearities present in the system. This process includes visualizing these nonlinearities using the ASM to aid in selecting the most appropriate mathematical form for modeling each nonlinearity accurately. Finally, with the model selected, parameter estimation is carried out based on the governing equations of motion, identifying the nonlinear coefficients through the RFS method. Depending on the model's complexity, the parameters are then estimated using either linear least-squares fitting or nonlinear optimization algorithms, ensuring an accurate representation of the nonlinear effects within the system.

2.1 Detection of Nonlinearity

Detection is conducted through various tests, detailed in Appendix A. During these tests, a linear sine-sweep excitation is used. This method is chosen for its deterministic nature, ease of visual interpretation, and strong activation of nonlinearities due to concentrated energy within the bandwidth of interest.

The first approach involves comparing the frequency response of the linear structure, shown in Figure 1.1, to that of the studied structure. The frequency response of both systems is presented in Figure 2.2. Nonlinear behavior is observed around the second resonance frequency, between



27.57 Hz and 30.85 Hz. Additionally, the jump at 30.3 Hz indicates a potentially marked increase in stiffness, confirming the presence of nonlinear dynamics within the system. The asymmetry in amplitude variation around the second resonance frequency further emphasizes the nonlinear characteristics of the structure.

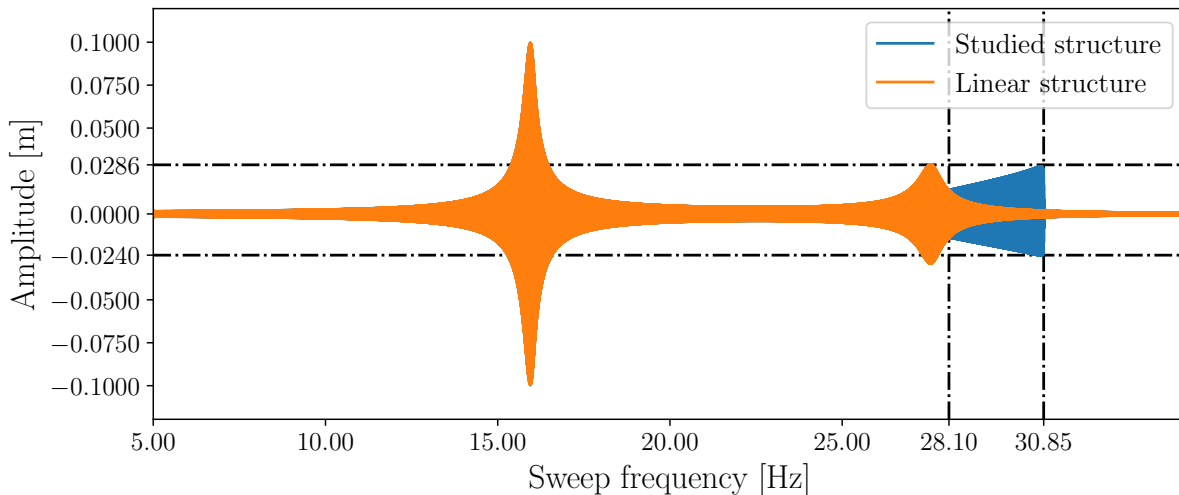


Figure 2.2: Comparison of the frequency response of DOF 2 under a sine sweep of 40 N applied to DOF 1 (Experiment 1, Test 1), representing the studied structure, with the linear structure shown in Figure 1.1.

The second approach examines the frequency response function across different excitation amplitudes to identify the point at which the principle of superposition, a cornerstone of linear vibration theory, no longer applies. This analysis is illustrated in Figure 2.3. Distinct variations in the shape of the frequency response function (FRF), particularly near the second resonance peak, indicate that the principle of superposition does not hold in these regions. An observable shift of the resonance towards higher frequencies with increasing amplitude further confirms the growth in stiffness.

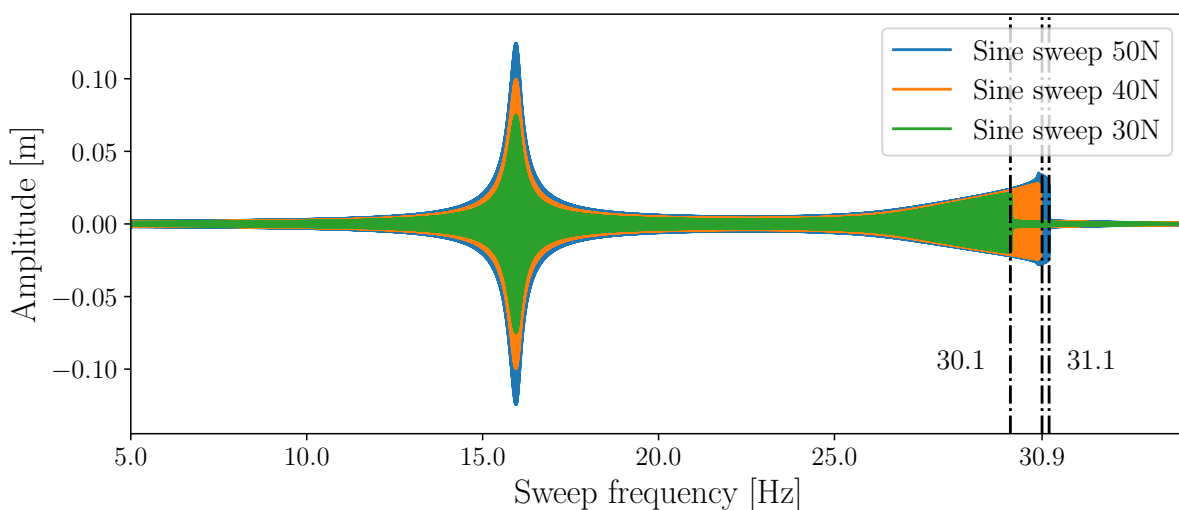


Figure 2.3: Comparison of sine sweeps for different forcing amplitudes (30, 40, 50 N) applied to DOF 1 (Experiment 2), measured at DOF 2.

The final approach involves reversing the direction of the sine sweep to assess response consistency. In a perfectly linear system, responses from both directions would align closely,



with any minor discrepancies arising due to transient effects from the non-stationary excitation [6]. This method helps highlight potential nonlinearities, as illustrated in Figure 2.4. Two distinct types of nonlinearity, as observed previously, are evident in the system: the amplitude jump near the second resonance peak, and the asymmetry along the x-axis.

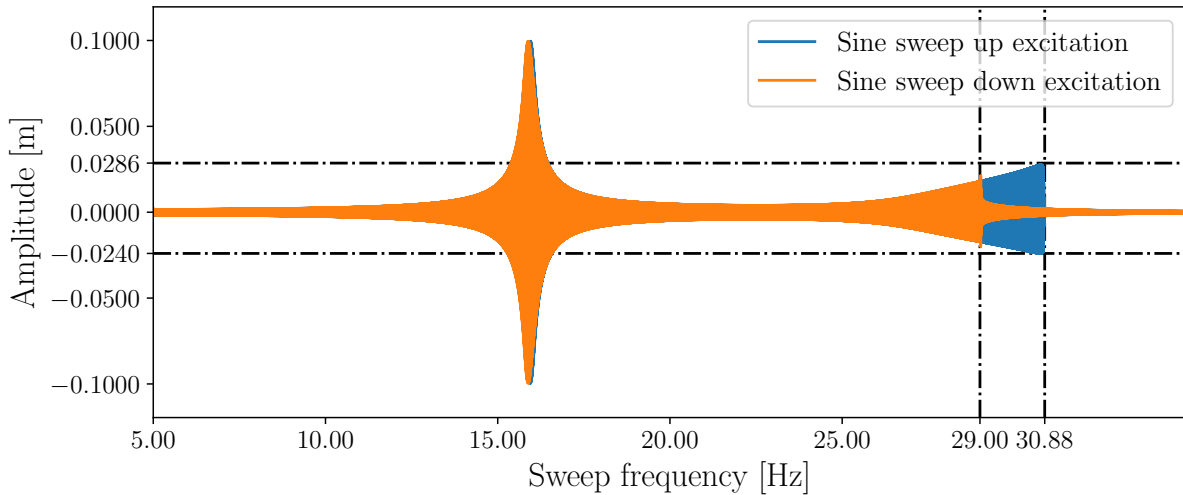


Figure 2.4: Comparison of upward and downward sine sweep excitations applied to DOF 1 and measured on DOF 2, represented by Experiment 1, Tests 1 and 2.

2.2 Characterization of Nonlinearity

The second step focuses on pinpointing the location of the nonlinearity, analyzing the underlying physical mechanisms, and establishing a functional representation of the nonlinear forces $f_{nl}(q, \dot{q})$. A common approach is to identify the functional form of these forces is the ASM, a simplified variant of the RFS method [4, 5].

2.2.1 Determine the Nonlinearity Location

Following the detection of non-linearity, the location of the non-linearity in the system can be determined. Considering that this is a 2-DoFs system, the following characteristics are observed in each mode:

- **First Mode:** The two masses move together in the same direction, meaning there is no relative displacement between them. This mode primarily engages the springs and dampers that connect each mass to the ground.
- **Second Mode:** The masses move in opposite directions, creating significant relative displacement between them. Consequently, this mode strongly engages the springs and dampers between the two masses.

As the first mode exhibits no nonlinearity, whereas the second mode does, the nonlinearity is likely located between the two masses rather than between an individual mass and the ground.

2.2.2 Acceleration Surface Method (ASM)

The ASM relies solely on acceleration measurements obtained at the two endpoints, i and j , of a nonlinear connection, as illustrated in Figure 2.5.

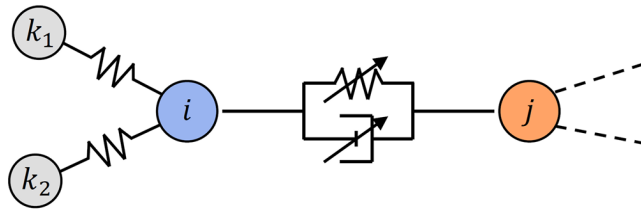


Figure 2.5: Nonlinear connection with assumed endpoints i and j for the ASM [8].

In the general case, velocity and displacement can be derived from acceleration through integration, typically performed using the trapezoidal rule combined with high-pass filtering [19]¹. This method relies on a few assumptions [17]:

- linear or negligible contributions from the surrounding connections,
- small damping forces around zero relative velocity,
- only one mode responding at a time.

The ASM is derived from Newton's second law applied to the degree of freedom i , leading to the following general equation:

$$\sum_k m_{i,k} \ddot{q}_k + g_i(q, \dot{q}) = p_i, \quad (2.1)$$

where $m_{i,k}$ represents the (i, k) -th element of the mass matrix \mathbf{M} , q_k is the displacement of the degree of freedom k , g_i denotes the internal force acting on the degree of freedom i , and p_i is the external force applied to i .

In this formulation, only the terms related to the nonlinear connection between the degrees of freedom i and j are retained, simplifying the equation to:

$$m_{i,i} \ddot{q}_i + g_i(q_i - q_j, \dot{q}_i - \dot{q}_j) \approx p_i. \quad (2.2)$$

The external force is neglected, and the mass $m_{i,i}$ is omitted, as it acts as a simple scaling factor [5]. This simplifies the equation to:

$$g_i(q_i - q_j, \dot{q}_i - \dot{q}_j) \approx -\ddot{q}_i. \quad (2.3)$$

The force g_i , representing the combined stiffness and damping forces between degrees of freedom i and j , is assumed to be nonlinear. It can therefore be approximated by the negative acceleration at degree of freedom i . The ASM consists of representing the acceleration $-\ddot{q}_i$ as a function of the relative displacement $q_i - q_j$ and the relative velocity $\dot{q}_i - \dot{q}_j$, creating a three-dimensional surface of the acceleration.

The surface can also be projected into a two-dimensional representation by plotting the acceleration as a function of the relative displacement when $\dot{q}_i - \dot{q}_j = 0$, and as a function of the relative velocity when $q_i - q_j = 0$. These plots are referred to as the stiffness curve and the damping curve, respectively. They provide valuable insights into the functional behavior of the stiffness and damping forces in the nonlinear connection. These curves are then analyzed to identify potential nonlinearities in the stiffness or damping forces and to develop appropriate mathematical models for their representation. The acceleration surface, along with the stiffness

¹In this case, this value is given in the experience



and damping curves, are depicted in Figure 2.6. This method is applied only to the second mode for clarity, assuming that the first mode does not exhibit any nonlinear effects.

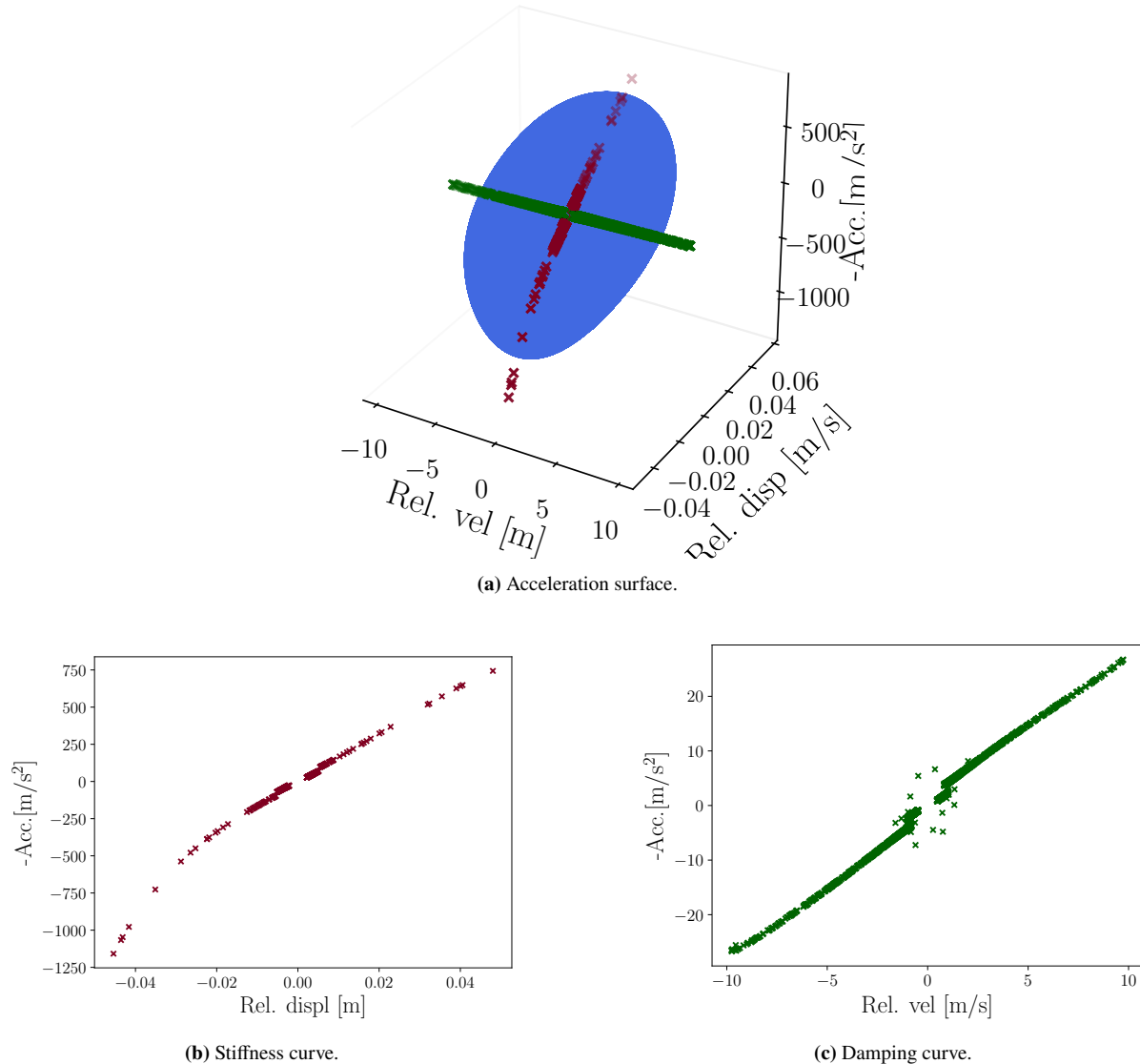


Figure 2.6: Acceleration surface and stiffness and damping curve for DoF 2 focusing on the second mode, data use experience 1 test 1.

The acceleration measured corresponds to the second degree of freedom, consistent with the assumptions of the ASM, where no external forces act on the degree of freedom of the measured acceleration. When examining the stiffness and damping curves, it is observed that the stiffness curve can be closely approximated by a polynomial function due to its smooth character and lack of discontinuities. On the other hand, the damping curve's relatively small magnitude compared to the stiffness curve, along with its better fit to a linear function, indicates the absence of significant nonlinear damping forces. Additionally, near the origin, the points appear to be randomly distributed and concentrated near the center of the curve. These points originate from regions after the resonance peak and are therefore excluded from this analysis [5].



2.3 Parameter Estimation

The final step in nonlinear system identification is parameter estimation, which can be achieved using the RFS method [5, 7]. This method serves as the generalized form of the ASM approach, from which it is derived [5]. The primary objective is to determine the parameters of the nonlinear model based on the functional form of the nonlinear forces identified in the previous section.

According to Newton's second law, the system dynamics are expressed as:

$$\mathbf{M}\ddot{\mathbf{q}} + \mathbf{C}\dot{\mathbf{q}} + \mathbf{K}\mathbf{q} + \mathbf{f}_{\text{nl}}(\mathbf{q}, \dot{\mathbf{q}}) = \mathbf{p}(t), \quad (2.4)$$

where $\mathbf{p}(t)$ represents the external forces applied to the system, and \mathbf{f}_{nl} denotes the nonlinear forces that depend on the displacement \mathbf{q} and velocity $\dot{\mathbf{q}}$. This equation can be rewritten in a more convenient form for analysis and estimation:

$$\mathbf{f}_{\text{nl}}(\mathbf{q}, \dot{\mathbf{q}}) = \mathbf{p}(t) - \mathbf{M}\ddot{\mathbf{q}} - \mathbf{C}\dot{\mathbf{q}} - \mathbf{K}\mathbf{q}, \quad (2.5)$$

where \mathbf{M} , \mathbf{K} , and \mathbf{C} are known, and $\mathbf{p}(t)$, along with $\ddot{\mathbf{q}}, \dot{\mathbf{q}}, \mathbf{q}$, are obtained from experimental measurements. This allows for the calculation of $\mathbf{f}_{\text{nl}}(\mathbf{q}, \dot{\mathbf{q}})$. Assuming a functional form for the nonlinear restoring force derived during the characterization step, an estimate of the nonlinear force can be expressed as:

$$\hat{\mathbf{f}}_{\text{nl}}(\mathbf{q}, \dot{\mathbf{q}}) = \sum_{i=1}^M k_i \mathbf{f}_i(\mathbf{q}, \dot{\mathbf{q}}), \quad (2.6)$$

where $\mathbf{f}_i(\mathbf{q}, \dot{\mathbf{q}})$ are the M assumed functional forms of the nonlinear force, and k_i are the M parameters to be estimated using the RFS method. Based on this representation of the nonlinear force, the governing equation can be reformulated as:

$$[\mathbf{f}_1(\mathbf{q}, \dot{\mathbf{q}}) \quad \cdots \quad \mathbf{f}_M(\mathbf{q}, \dot{\mathbf{q}})] \begin{bmatrix} k_1 \\ \vdots \\ k_M \end{bmatrix} = \mathbf{p}(t) - \mathbf{M}\ddot{\mathbf{q}} - \mathbf{C}\dot{\mathbf{q}} - \mathbf{K}\mathbf{q} \quad (2.7)$$

Knowing the external force $\mathbf{p}(t)$ and the displacement \mathbf{q} , velocity $\dot{\mathbf{q}}$, and acceleration $\ddot{\mathbf{q}}$ at Q different times t_1, \dots, t_Q , with $Q > M$ [5]. An overdetermined system of equations is obtained:

$$\begin{bmatrix} \mathbf{f}_1(\mathbf{q}(t_1), \dot{\mathbf{q}}(t_1)) & \cdots & \mathbf{f}_M(\mathbf{q}(t_1), \dot{\mathbf{q}}(t_1)) \\ \vdots & \ddots & \vdots \\ \mathbf{f}_1(\mathbf{q}(t_Q), \dot{\mathbf{q}}(t_Q)) & \cdots & \mathbf{f}_M(\mathbf{q}(t_Q), \dot{\mathbf{q}}(t_Q)) \end{bmatrix} \begin{bmatrix} k_1 \\ \vdots \\ k_M \end{bmatrix} = \begin{bmatrix} \mathbf{p}(t_1) - \mathbf{M}\ddot{\mathbf{q}}(t_1) - \mathbf{C}\dot{\mathbf{q}}(t_1) - \mathbf{K}\mathbf{q}(t_1) \\ \vdots \\ \mathbf{p}(t_Q) - \mathbf{M}\ddot{\mathbf{q}}(t_Q) - \mathbf{C}\dot{\mathbf{q}}(t_Q) - \mathbf{K}\mathbf{q}(t_Q) \end{bmatrix},$$

for which the parameters k_i are the unknowns. The least-squares solution of this system of equations is given by:

$$\begin{bmatrix} k_1 \\ \vdots \\ k_M \end{bmatrix} = \left[\mathbf{f}_1(\mathbf{q}(t_1), \dot{\mathbf{q}}(t_1)) \quad \cdots \quad \mathbf{f}_M(\mathbf{q}(t_1), \dot{\mathbf{q}}(t_1)) \right]^\dagger \begin{bmatrix} \mathbf{p}(t_1) - \mathbf{M}\ddot{\mathbf{q}}(t_1) - \mathbf{C}\dot{\mathbf{q}}(t_1) - \mathbf{K}\mathbf{q}(t_1) \\ \vdots \\ \mathbf{p}(t_Q) - \mathbf{M}\ddot{\mathbf{q}}(t_Q) - \mathbf{C}\dot{\mathbf{q}}(t_Q) - \mathbf{K}\mathbf{q}(t_Q) \end{bmatrix}.$$

Based on the results of the ASM, the nonlinear force is assumed to be a polynomial function that depends on the relative displacement. As previously stated, the nonlinear force is assumed to act between the two degrees of freedom. As a result, it is independent of the displacement or



velocity of any individual degree of freedom and depends solely on the relative displacement between both. The coefficients of the nonlinear force and the appropriate order of its polynomial representation, initially unknown, were determined by progressively increasing the polynomial order. This process continued until the mean square error (MSE) indicated an adequate level of accuracy [7], ensuring that all terms of the polynomial contributing to the nonlinear force were accounted for. The nonlinear force components were represented using the functional form:

$$\mathbf{f}_i = \begin{bmatrix} -(q_2 - q_1)^i \\ (q_2 - q_1)^i \end{bmatrix}. \quad (2.8)$$

The force acting on each node has an opposite sign, ensuring that the sum of the nonlinear forces acting on the two degrees of freedom is equal to zero. Since this force is located between the two masses, it is an internal force within the system. Consequently, the sum of all internal forces on the system must also be equal to zero, in accordance with the principles of mechanics.

To determine the contribution of each coefficient, the significance factor [1] is defined as:

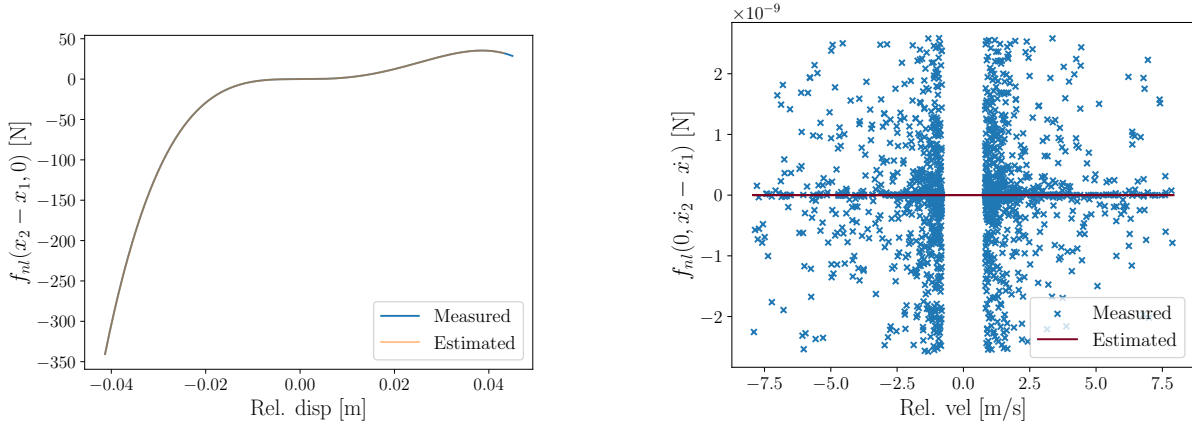
$$s_\theta = 100 \frac{\sigma_\theta^2}{\sigma_x^2}, \quad (2.9)$$

where σ_x^2 represents the variance of the sum of all terms in the model, and σ_θ^2 corresponds to the variance of the specific term under consideration. This factor quantifies the percentage contribution of each term to the total variance of the model.

Using this approach, only the coefficients for terms of order 3, 4, and 7 were retained, resulting in the following expression for the nonlinear force components:

$$\hat{\mathbf{f}}_{nl}(\mathbf{q}, \dot{\mathbf{q}}) = \begin{bmatrix} -2.6 \times 10^6 (q_2 - q_1)^3 + 5.2 \times 10^7 (q_2 - q_1)^4 - 1.9 \times 10^{10} (q_2 - q_1)^7 \\ 2.6 \times 10^6 (q_2 - q_1)^3 - 5.2 \times 10^7 (q_2 - q_1)^4 + 1.9 \times 10^{10} (q_2 - q_1)^7 \end{bmatrix}. \quad (2.10)$$

To validate these results, the nonlinear force as a function of relative displacement, when $\dot{q}_2 - \dot{q}_1 = 0$, is shown in Figure 2.7a. The estimated force using the RFS method closely matches the measured data, confirming the nonlinear force behavior. Similarly, Figure 2.7b presents the nonlinear force as a function of relative velocity, when $q_2 - q_1 = 0$. The measured values are observed to be very small and do not follow a specific trajectory. This supports the hypothesis that the nonlinear force is not influenced by relative velocity.



(a) Comparison between the nonlinear force as a function of relative displacement at zero relative velocity.

(b) Comparison of the nonlinear force as a function of relative velocity at zero relative displacement.

Figure 2.7: Nonlinear force measured and estimated at DOF2 using the RFS method. The results are shown as a function of relative displacement when $\dot{q}_2 - \dot{q}_1 = 0$ and as a function of relative velocity when $q_2 - q_1 = 0$. Only the force at DoF 2 is considered, with the estimated force for relative velocity being zero due to the assumption of no damping in the system.



3 Simulation of the Nonlinearity

The simulation of nonlinearity will be based on nonlinear frequency responses and nonlinear normal modes. These will be determined using a shooting method combined with sequential continuation.

3.1 Nonlinear Frequency Responses (NLFRs)

NLFRs curves are obtained by computing branches of the periodic solutions of the damped model under harmonic excitation. These curves are particularly useful as they describe the evolution of the amplitude of the steady-state responses of the structure, *i.e.* after the transients.

It is important to note that, in the presence of nonlinearity, the principles of superposition and uniqueness do not apply. Additionally, the NLFRs are energy-dependent and can exhibit both stable and unstable branches, depending on the system's dynamics.

3.1.1 NLFRs Calculation

NLFRs are calculated using a shooting method combined with sequential continuation. The shooting method [13, 15] is derived for a system of second-order ordinary differential equations [16]. It is assumed that the external force is harmonic, and therefore, the period of vibration is considered known. The vector of generalized displacements and velocities depends on time t , as well as on the initial conditions \mathbf{q}_0 and $\dot{\mathbf{q}}_0$, which correspond to a periodic motion. For this purpose, Equation 2.4 is reformulated as a boundary value problem:

$$\dot{\mathbf{y}}(t) = L\mathbf{y}(t) - \mathbf{g}_{\text{nl}}(\mathbf{y}) + \mathbf{g}_{\text{ext}}(\omega, t) \quad (3.1)$$

with :

$$\begin{aligned} \mathbf{y} &= \begin{bmatrix} \mathbf{x} \\ \dot{\mathbf{x}} \end{bmatrix}, \quad L = \begin{bmatrix} 0 & I_n \\ -M^{-1}K & -M^{-1}C \end{bmatrix}, \\ \mathbf{g}_{\text{nl}} &= \begin{bmatrix} 0 \\ M^{-1}f_{\text{nl}}(\mathbf{x}, \dot{\mathbf{x}}) \end{bmatrix}, \quad \mathbf{g}_{\text{ext}} = \begin{bmatrix} 0 \\ M^{-1}f_{\text{ext}}(\omega, t) \end{bmatrix}. \end{aligned}$$

The objective of the method is to determine the initial conditions such that

$$\mathbf{y}(T, \mathbf{y}_{0,p}^n) = \mathbf{y}(0, \mathbf{y}_{0,p}^n), \quad (3.2)$$

where T represents the minimal period of vibration determined by the excitation frequency. This is achieved through an iterative process, as illustrated in Figure 3.1.

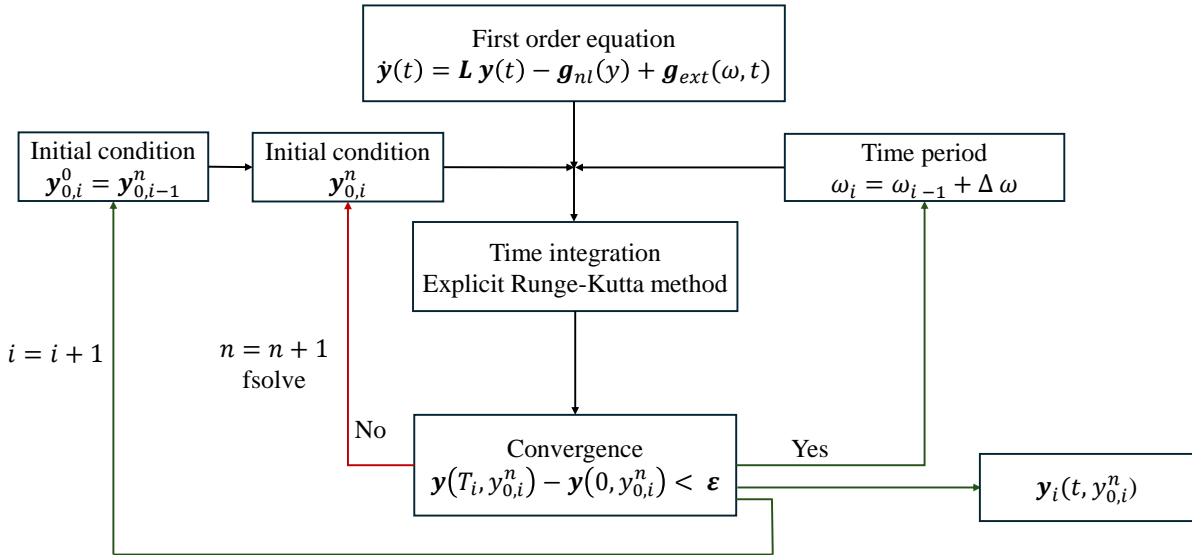


Figure 3.1: Shooting method with a sequential continuation.

The objective is to determine the root of the function

$$h = \mathbf{y}(T, \mathbf{y}_{0,p}^n) - \mathbf{y}(0, \mathbf{y}_{0,p}^n), \quad (3.3)$$

by adjusting only the initial condition $\mathbf{y}_{0,p}$. The shooting method begins with an initial guess (predictor) for the initial conditions, which is defined based on the solution obtained earlier from the sequential continuation process.

An explicit fourth-to-fifth-order Runge-Kutta method is used to solve the ordinary differential equation. This method offers a good balance between accuracy and computational cost. For root-finding, Powell's Hybrid Method [14] is used.

Another aspect of the method involves the sequential-type continuation algorithm. This approach is designed to compute FRCs by calculating the response at each period with a specific time step, defined as $\omega_i = \omega_{i-1} + \Delta\omega$. However, a significant limitation of this method arises at turning points, encounters difficulties in accurately tracking the curve. This limitation restricts its ability to capture all possible solutions. In such cases, more advanced continuation strategies, such as the pseudo-arclength scheme [3], may be required to obtain reliable and comprehensive results.

To address this limitation, the frequency is inverted, starting from the end and progressing toward the beginning. This adjustment aims to capture all possible frequency responses.

3.1.2 NLFs Representation

The simulated frequency range is [10, 35] Hz to capture all the features of the obtained curves. The system is simulated under force amplitudes of 10, 30, and 50 N to investigate the response in greater detail as a function of amplitude². The results are presented in Figure 3.2.

²Since the principle of superposition does not apply, it is crucial to analyze the response for different amplitudes.

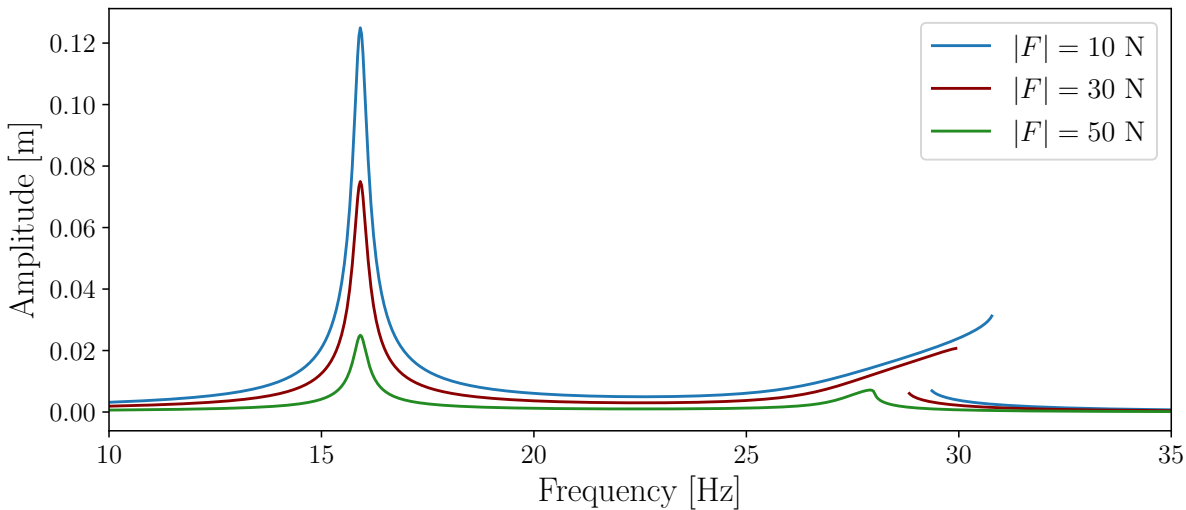


Figure 3.2: Nonlinear Frequency Responses (NLFRs) simulation of DoF 2 for three different amplitudes applied to DoF 1.

It can be observed that the shape of the first mode remains unchanged compared to the initial state. This is expected, as the applied force predominantly affects the second mode. At $F = 10$ N, the nonlinearity is barely noticeable; however, as the amplitude increases, the nonlinear nature of the response becomes more pronounced. The system exhibits hardening behavior, but at higher forces, such as $F = 50$ N, as the frequency moves further away from the peak, a softening effect is observed. This behavior is attributed to the dominance of the seventh-order term of the $\hat{\mathbf{f}}_{\text{nl}}(\mathbf{q}, \dot{\mathbf{q}})$, which outweighs the contribution of the lower-order terms. Additionally, the turning point is clearly visible, and as discussed earlier, the continuation algorithm fails to follow the curve beyond this point, resulting in a jump in the response.

3.1.3 NLFRs Validation

For validation, the software *NI2D* [17], which incorporates a harmonic balance continuation algorithm, is used alongside the testing results from an upward and downward sine sweep.

The comparison with *NI2D* is shown in Figure 3.3. The harmonic balance method, being a more advanced technique, is capable of continuing the solution even in the presence of bifurcations. It can be observed that the shooting method converges; however, at high amplitudes, the turning point appears earlier than expected, due to the loop at the end of the peak is not fully captured by the shooting method. This loop is created by a hardening behavior followed by a softening effect, which generates the characteristic shape discussed in subsubsection 3.1.2.

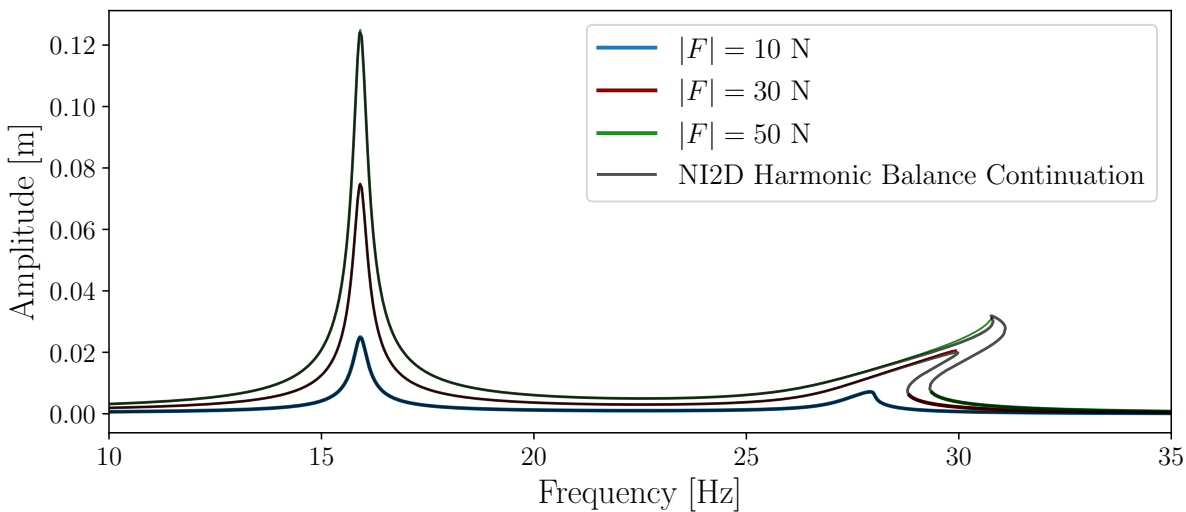


Figure 3.3: Comparison of the nonlinear response obtained using the shooting method with sequential continuation for DoF 2 under three different amplitudes applied to DoF 1, with results from a harmonic balance continuation algorithm extracted using the software *NI2D* [17].

The system's response is further validated using a sine sweep forcing function. This approach applies a sinusoidal excitation at each frequency of interest with a constant amplitude. It is particularly useful for system identification, but can also serve as a method to validate the results. Similar to the shooting method with sequential continuation, the sine sweep is applied in both ascending and descending frequency directions to observe hysteresis effects, as illustrated in Figure 3.4.

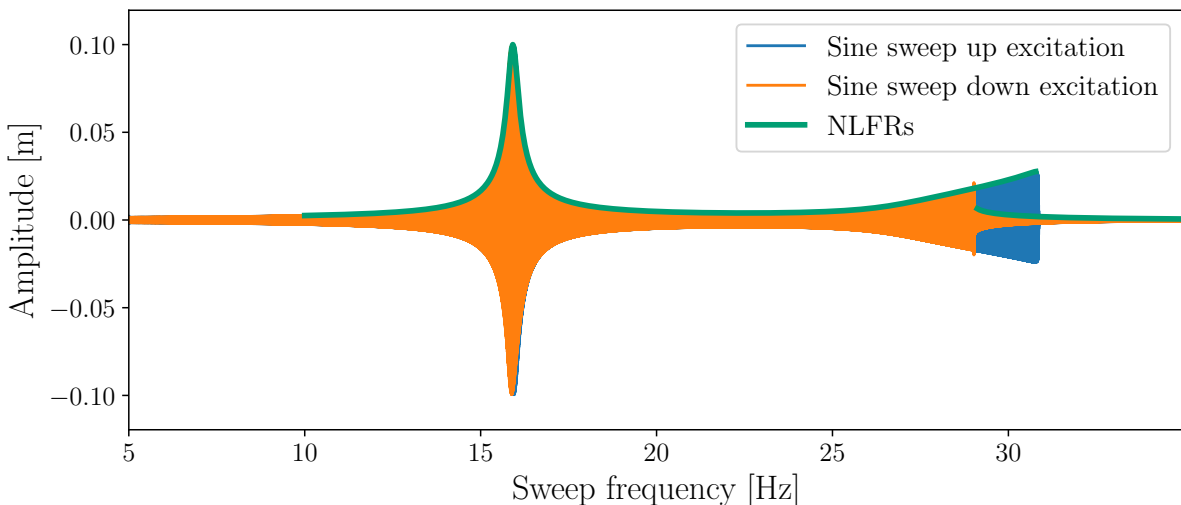


Figure 3.4: Validation of experimental data (Experiment 1, Tests 1 and 2) with the NLFRs of DoF 2 for a forcing amplitude of 40 N at DoF 1.

It can be observed that the NLFRs behave as expected. The upward sine sweep matches perfectly with the NLFRs until the turning point, but beyond this point, the sine sweep curve continues while the NLFR trace fades out. This slight discrepancy can be attributed to the properties of the sine sweep [6]. It can also be noted that after the turning point, the NLFRs align with the downward sine sweep, confirming the anticipated behavior.



3.2 Nonlinear Normal Modes (NNMs)

NNMs [9] are obtained by computing the branches of periodic solutions underlying the undamped and unforced model:

$$\mathbf{M}\ddot{\mathbf{q}} + \mathbf{K}\mathbf{q} + \mathbf{f}_{\text{nl}}(\mathbf{q}, \dot{\mathbf{q}}) = 0. \quad (3.4)$$

eNNMs are particularly useful as they describe the deformation of the structure at resonance and illustrate how the modal parameters evolve with the motion amplitude. To highlight the frequency-amplitude dependence in nonlinear oscillations, the backbone curve is one of the most effective tools. Another approach involves analyzing the energy-frequency dependence, although this aspect is not addressed in the scope of this project.

3.2.1 Backbone Curve

Backbone curves are a powerful tool for analyzing nonlinear systems [18, 20]. These curves illustrate the natural frequency as a function of the system's response amplitude under conditions free of damping and external forces. They provide a detailed representation of system dynamics, allowing for the identification and quantification of nonlinearities. In addition, they expose internal interactions within the system, such as modal energy exchanges induced by nonlinear effects, which are not observable through traditional linearized methods [12]. Backbone curves also serve as a means to identify or refine the nonlinear characteristics of a model using experimental data [2, 11]. In this project, the backbone curve is computed using the shooting method with sequential continuation, as illustrated in Figure 3.1, which provides a schematic representation of the method. The calculation focuses on the second mode, where nonlinearity is present. The resulting backbone curve is compared to the one extracted from NI2D [17] and is presented in Figure 3.5.

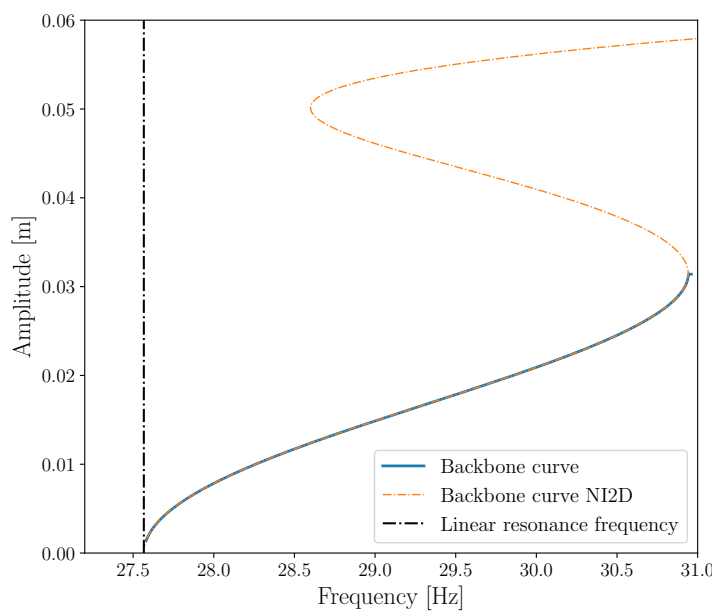


Figure 3.5: Backbone curve of the second mode compared to the one obtained using NI2D [17].

The hardening and softening behaviors are particularly visible in this representation. For the results obtained with NI2D, it can be observed that a hardening behavior follows the softening behavior. However, determining the initial conditions for the shooting method is challenging.



Two approaches can be considered: the first involves using *NI2D* [17] to simulate the initial conditions, while the second relies on determining them based on prior knowledge that at 27.57 Hz, the starting point of the backbone corresponds to the resonance frequency of the linear system.

Nevertheless, starting from this resonance frequency often causes the shooting process to converge to a trivial solution, consistently returning null values. Additionally, after reaching a certain limit, the shooting method identifies a bifurcation point, likely linked to the shape of the response at $F = 50$ N, which creates a loop that the algorithm struggles to follow.

The backbone curve, as shown in Figure 3.6, represents the maximum amplitude of each NLFR for varying forcing levels. For $F = 10$ N and $F = 30$ N, the backbone aligns well with the NLFRs. However, at $F = 50$ N, the backbone fails to intersect the response curve, likely due to the complex shape of the NLFRs at this amplitude, as evidenced by the results obtained with *NI2D* in Figure 3.3.

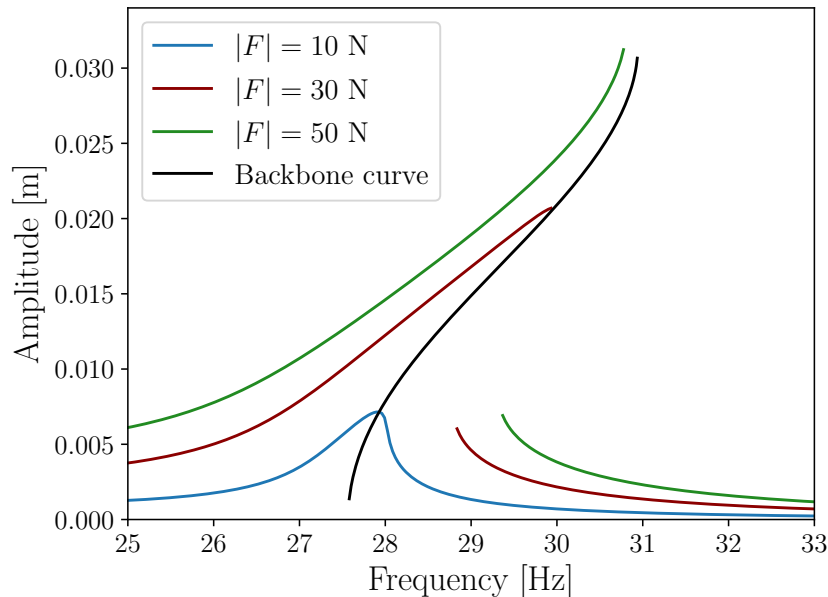


Figure 3.6: Superposition of the backbones curve and the NLFRs at three different forcing amplitudes 10,30,50 N



4 Conclusion

The project successfully addressed the challenge of identifying and simulating nonlinearities in a two-degree-of-freedom mechanical system, commonly encountered in aerospace and mechanical structures. The approach was divided into two main phases: the identification of nonlinearities and their subsequent simulation.

In the identification phase, the parameters of the nonlinearities within the system were systematically detected, characterized, and estimated. The detection process revealed significant nonlinear behaviors, particularly in the second resonance mode, using frequency response functions and sine-sweep techniques. Characterization using the Acceleration Surface Method (ASM) provided both visual and mathematical representations of the nonlinear stiffness and damping forces. This approach pinpointed the location of the nonlinear elements, showing a polynomial behavior for the stiffness and a linear behavior for the damping. For the second mode, the Restoring Force Surface (RFS) method was applied to model the stiffness as a polynomial function. By incrementally increasing the polynomial order and analyzing the mean-square error, the nonlinear force component was identified as:

$$\hat{\mathbf{f}}_{\text{nl}}(\mathbf{q}, \dot{\mathbf{q}}) = \begin{bmatrix} -2.6 \times 10^6(q_2 - q_1)^3 + 5.2 \times 10^7(q_2 - q_1)^4 - 1.9 \times 10^{10}(q_2 - q_1)^7 \\ 2.6 \times 10^6(q_2 - q_1)^3 - 5.2 \times 10^7(q_2 - q_1)^4 + 1.9 \times 10^{10}(q_2 - q_1)^7 \end{bmatrix}.$$

In the simulation phase, advanced numerical techniques were employed, such as the shooting method combined with sequential continuation. This approach enabled the generation of Nonlinear Frequency Responses (NLFRs), which captured the system's behavior under varying excitation amplitudes. A clear hardening and softening behavior emerged at higher amplitudes. To validate this method, the software *NI2D* was used, this software incorporates harmonic balance continuation to detect bifurcations. Furthermore, the NLFRs obtained from this approach were compared with sine-sweep up and sine-sweep down methods, demonstrating high accuracy. Additionally, Nonlinear Normal Modes (NNMs) were analyzed using the backbone curve to highlight the intrinsic frequency-amplitude relationship of the system, offering deeper insights into its nonlinear dynamics. The backbone curve effectively illustrated the connection between NNMs and NLFRs, showcasing the beauty of nonlinear behavior. Notably, the system failed to intersect at an amplitude of 50 N, due to the complex shapes of the NLFR amplitude caused by the softening behavior observed.

This study not only provides a comprehensive understanding of the nonlinear phenomena in the system but also establishes a robust framework for analyzing and predicting complex dynamics in aerospace and mechanical applications. The methods and results contribute significantly to advancing reliable modeling techniques, which are critical for designing robust systems.



A Experimental Setup Parameters

A.1 Experimental 1

	Test 1	Test 2	Test 3
Type	Sine sweep	Sine sweep	Sine sweep
Forced dof(s)	1	1	1
Amplitude [N]	40	40	0
Starting frequency [Hz]	5	35	5
Ending frequency [Hz]	35	5	45
Sweep rate [Hz/min]	1	1	1
Sweep style	Linear	Linear	Linear
Newmark Solver Parameters			
Time step [sec]	1.1×10^{-4}	1.1×10^{-4}	1.1×10^{-4}
Initial time [sec]	0	0	0

Table A.1: External force and setup for the first experiment. The objective is to perform an upward and downward sine sweep to observe non-linearities. These values are also used for comparison with the software *NI2D* [17].

A.2 Experimental 2

	Test 1	Test 2	Test 3
Type	Sine sweep	Sine sweep	Sine sweep
Forced dof(s)	1	1	1
Amplitude [N]	50	40	30
Starting frequency [Hz]	5	5	5
Ending frequency [Hz]	45	45	45
Sweep rate [Hz/min]	1	1	1
Sweep style	Linear	Linear	Linear
Newmark Solver Parameters			
Time step [sec]	1.1×10^{-4}	1.1×10^{-4}	1.1×10^{-4}
Initial time [sec]	0	0	0

Table A.2: External force and setup for the second experiment. The objective is to perform varying sine sweeps by adjusting only the amplitude to observe non-linearities.



A.3 Experimental 3

	Test 1	Test 2
Type	Sine	Sine
Forced dof(s)	1	1
Amplitude [N]	40	40
Frequency [Hz]	10	30
Phase [°]	0	0
Newmark Solver Parameters		
Time step [sec]	1.1×10^{-4}	1.1×10^{-4}
Initial time [sec]	0	0
Duration time [sec]	1	1

Table A.3: External force and setup for the third experiment. The objective is to apply a sinusoidal excitation at a specific frequency to validate the accuracy of the model.



References

- [1] P. Atkins and K. Worden. ‘Identification of a multi degree-of-freedom nonlinear system’. In: *Proceedings of the 15th International Modal Analysis Conference*. Vol. I. 1997, pp. 1023–1028.
- [2] A. Cammarano et al. ‘Nonlinear System Identification through Backbone Curves and Bayesian Inference’. In: *Nonlinear Dynamics*. Ed. by G. Kerschen. Vol. 1. Conference Proceedings of the Society for Experimental Mechanics Series. Switzerland: Springer International Publishing, 2015.
- [3] Jacob A. Dahlke and Robert A. Bettinger. ‘Practical implementation of pseudo-arclength continuation to ensure consistent path direction’. In: *Acta Astronautica* 215 (2024), pp. 205–216. ISSN: 0094-5765. doi: <https://doi.org/10.1016/j.actaastro.2023.12.007>. URL: <https://www.sciencedirect.com/science/article/pii/S0094576523006379>.
- [4] T. Dossogne et al. ‘Nonlinear dynamic model upgrading and updating using sine-sweep vibration data’. In: *Proceedings of the Royal Society A* 475 (2019).
- [5] F. Ghysens. ‘Master thesis and internship: Assessing the robustness of the acceleration surface method’. Unpublished master’s thesis. Liège, Belgique: Université de Liège, 2024. URL: <https://matheo.uliege.be/handle/2268.2/20237>.
- [6] G. Gloth and M. Sinapius. ‘Analysis of swept-sine runs during modal identification’. In: *Mechanical Systems and Signal Processing* 18.6 (2004), pp. 1421–1441. ISSN: 0888-3270. doi: [https://doi.org/10.1016/S0888-3270\(03\)00087-6](https://doi.org/10.1016/S0888-3270(03)00087-6). URL: <https://www.sciencedirect.com/science/article/pii/S0888327003000876>.
- [7] G. Kerschen, J.-C. Golinval and K. Worden. ‘Theoretical and experimental identification of a non-linear beam’. In: *Journal of Sound and Vibration* 244.4 (2001), pp. 597–613. doi: [10.1006/jsvi.2000.3490](https://doi.org/10.1006/jsvi.2000.3490). URL: <http://www.idealibrary.com>.
- [8] G. Kerschen and G. Raze. *Nonlinear vibrations of aerospace structures - Lecture notes*. University of Liège, 2024.
- [9] G. Kerschen et al. ‘Nonlinear Normal Modes, Part I: An Attempt To Demystify Them’. In: *Unknown* (2009). Structural Dynamics Research Group, Department of Aerospace and Mechanical Engineering.
- [10] G. Kerschen et al. ‘Past, present and future of nonlinear system identification in structural dynamics’. In: *Mechanical Systems and Signal Processing* 20.3 (2006), pp. 505–592.
- [11] J.M. Londoño, S.A. Neild and J.E. Cooper. ‘Systems with Bilinear Stiffness: Extraction of Backbone Curves and Identification’. In: *Nonlinear Dynamics*. Ed. by G. Kerschen. Vol. 1. Conference Proceedings of the Society for Experimental Mechanics Series. Switzerland: Springer International Publishing, 2015. doi: [10.1007/978-3-319-15221-9_27](https://doi.org/10.1007/978-3-319-15221-9_27). URL: [http://dx.doi.org/10.1007/978-3-319-15221-9_27](https://dx.doi.org/10.1007/978-3-319-15221-9_27).
- [12] Julián M. Londoño, Simon A. Neild and Jonathan E. Cooper. ‘Identification of backbone curves of nonlinear systems from resonance decay responses’. In: *Journal of Sound and Vibration* 348 (2015), pp. 224–238. ISSN: 0022-460X. doi: <https://doi.org/10.1016/j.jsv.2015.03.015>. URL: <https://www.sciencedirect.com/science/article/pii/S0022460X15002333>.
- [13] Ali H. Nayfeh and Balakumar Balachandran. *Applied Nonlinear Dynamics: Analytical, Computational, and Experimental Methods*. New York: John Wiley & Sons, Inc., 1995.



- [14] M. J. D. Powell. ‘A hybrid method for nonlinear equations’. In: *Numerical Methods for Nonlinear Algebraic Equations*. 1970.
- [15] Rüdiger Seydel. *Practical Bifurcation and Stability Analysis*. 3rd. New York: Springer, 2010.
- [16] S. Stoykov and S. Margenov. ‘Numerical computation of periodic responses of non-linear large-scale systems by shooting method’. In: *Computers Mathematics with Applications* 67.12 (2014). Efficient Algorithms for Large Scale Scientific Computations, pp. 2257–2267. ISSN: 0898-1221. doi: <https://doi.org/10.1016/j.camwa.2014.01.023>. URL: <https://www.sciencedirect.com/science/article/pii/S0898122114000649>.
- [17] Département d’Ingénierie Université de Liège. *NI2D: Logiciel d’analyse des vibrations non linéaires*. 2024.
- [18] D.J. Wagg and S.A. Neild. *Nonlinear Vibration with Control*. Vol. 170. Solid Mechanics and Its Applications. Dordrecht, The Netherlands: Springer-Verlag, 2010.
- [19] K. Worden. ‘Data processing and experiment design for the restoring force surface method, part I: integration and differentiation of measured time data’. In: *Mechanical Systems and Signal Processing* 4 (1990), pp. 295–319.
- [20] K. Worden and G. Tomlinson. *Nonlinearity in Structural Dynamics: Detection, Identification and Modelling*. Bristol, Philadelphia: IOP Publishing Ltd, 2001.